The Effects of Atmospheric Compensation Upon Gaseous Plume Signatures

Benjamin L. Miller[a] and David W. Messinger[a]

[a]Digital Imaging and Remote Sensing Laboratory
Chester F. Carlson Center for Imaging Science
Rochester Institute of Technology

ABSTRACT

The usual first step in the processing of hyperspectral imagery is to remove the effects of the atmosphere. In the thermal region this usually involves accounting only for the upwelling radiance and the atmospheric transmission; the downwelling contribution being ignorable. This however can cause difficulties in the quantification of the gases if the atmosphere is improperly compensated for. Several algorithms exist for the compensation of the atmosphere including In-scene Atmospheric Compensation (ISAC) and Autonomous Atmospheric Correction (AAC). This study looks at which atmospheric compensation technique, if any, has the least negative impact on the gas signatures in the LWIR region (8-12 microns) using synthetic hyperspectral imagery created with the DIRSIG simulation. Two different metrics were used to this end: spectral angle and feature depth. Because the depth of the gas feature is directly related to the gas' concentration path length and temperature, it proved to be the more telling of the two. Results show that these atmospheric compensation routines have little effect in the strength of the gas features investigated here and, as such, atmospheric compensation may not be necessary.

Keywords: gas plumes, hyperspectral imagery, atmospheric compensation, AAC, ISAC, DIRSIG

1. INTRODUCTION

The problem of the detection, identification, and quantification of gaseous plume effluents is of importance not only to the remote sensing community but has applications in environmental monitoring as well. Success in detection and identification has been shown, in particular, using statistical agolrithms (PCA), matched filters, regression analysis, and the Invariant Algorithm.[1–3] The final step in the problem involves quantifying the temperature and the concentration of the gas and any mixing ratios. There has been some limited success with the quantification of the gases, but it a difficult problem.[4–6]

Most of the gases of interest in this problem have strong absorbtion/emission features in the long-wave infared (8-12 μm) and this is where the research has been focused. There are several issues that arise from the phenomena of the thermal regime. The gas, depending on the surface temperature constrast, may be in either absorption or emission. Also, some of the gases of interest are native to the atmosphere, such as ammonia. The feature strength, whether in absorption or emission, will depend on the concentration path length of the gas in question as well as the gas temperature. Finally, if there is spectral overlap of the gas with a native species it can complicate the problem.

Processing of hyperspectral imagery typically begins with the initial step of atmospheric compensation. Within the scope of the particular problem of identifying, detecting, and quantifying effluent gaseous plumes, identification and detection have been shown to be successful without the need for atmospheric compensation. For the problem of quantification though, the question of whether or not to preprocess the image with atmospheric compensation has been left open. By atmospherically compensating an image you affect productive or harmful changes to the spectral features which may lead to loss of information about the gas. These changes may be to the "strength" or the spectral "shape" of the feature. To this end, this paper is aimed at answering that question.

Further information: Chester F. Carlson Center for Imaging Science, Rochester Institute of Technology, 54 Lomb Memorial Dr., Rochester, NY 14623, blm7787@cis.rit.edu

2. ATMOSPHERIC COMPENSATION

Several atmospheric compensation algorithms exist for the LWIR region. The purpose is to transform at-sensor radiance into surface-leaving radiance by accounting for the atmospheric transmission and upwelling radiance only. The radiance equation for this model is

$$L(x,\lambda) = \tau(x,\lambda)L_s(x,\lambda) + L_p(x,\lambda) \tag{1}$$

where L is the at-sensor radiance, x is the pixel location, λ is the wavelength, L_s is the surface-leaving radiance, and L_p is the path radiance. Usually this is done to retrieve surface temperature and emissivity, though that is not the application here. Two algorithms were chosen for examination by this study: In-scene Atmospheric Compensation (ISAC) and Autonomous Atmospheric Compensation (ISAC).

2.1. In-Scene Atmospheric Compensation

The In-scene Atmospheric Compensation (ISAC) algorithm was developed by Young, *et. al* (2002), for specific use with the SEBASS[8] sensor. It is an empirical algorithm. It derives the atmospheric transmission and upwelled radiance from only the image data. It uses the 11.73 μm water vapor band only to estimate the scale of the atmospheric parameters. ISAC requires that the scene contains many blackbody pixels, not always a good assumption especially in the industrial and urban scenes that are the likely application for the gas problem. ISAC has the advantage that it is insensitive to instrument calibration errors and that it is widely availible. Here the IDL/ENVI implementation of ISAC was used.

2.2. Autonomous Atmospheric Compensation

The Autonomous Atmospheric Compensation (AAC) algorithm was developed by Gillespie, *et. al* (2000). It is a model based algorithm. It relates the two water band parameters that are derived from image data to statistics derived from 10,000 runs of MODTRAN. In this way AAC can match the shape and the scale of the atmospheric transmission and upwelled radiance. AAC requires that the emissivity curve near the water vapor band be smooth and close to unity. This is a good assumption if the background is vegetation or other natural materials and poor if it is of manmade materials. Unlike ISAC, AAC is vunerable to errors in instrument calibration. However, AAC produces local variable atmospheric parameters because the algorithm divides the image into segments (1024 pixels) and calculates individual transmission and upwelling for each.

3. EXPERIMENT DESIGN

To test the impact of each of the algorithms on plume data, synthetic imagery was used. The synthetic data has the advantage that the scene truth is known. The image data was generated through the use of DIRSIG, a synthetic scene generation tool that solves the full radiative transfer solution and involves radiation propagation through the plume. Here the data set that was used will be described and the metrics that were used to evaluate the algorithms will be explained.

3.1. Synthetic Data Set

The DIRS group has long delevoped and maintained a high-fidelity scene simulation tool: the **D**igital **I**maging and **R**emote **S**ensing **I**mage **G**eneration (DIRSIG) Model.[10] This is a first-principles ray trace model. A full three-dimensional model of the scene is created in a CAD environment. The facets of these objects are attributed with lab and field-measured physical and optical properties. Atmospheric contributions to the at-sensor radiance are modeled with MODTRAN.[11] A thermal model uses material properties as well as local weather and illumination history to perform sub-pixel temperature predictions. Several sensors can be simulated including framing arrays and line-scanners with multispectral and hyperspectral responses.

For the gaseuos effluent work, a three-dimensional Gaussian plume model can be included in the scene.[12] This model, while not spatially accurate (there are no "voids" or turbulence), does provide a three-dimensional representation of the plume concentration and temperature. Consequently, radiometric phenomology such as self absorption by the plume can be simulated. Required parameters for the plume simulation include values for

Figure 1. A single-band image of the synthetic DIRSIG data at 10.73 μm. This example is of the strong plume case. Both plumes can be seen in the image, starting in the center and moving to the lower right. The Freon-114 plume is the top-most plume and the ammonia plume is the bottom-most.

the gas absorption coefficient, the release rates and temperatures, the ambient air temperatures, and the stack height. A stepwise radiative transfer calculation is performed for those rays that transect the plume.

The DIRSIG tool allows the generation of scenes absence of any atmosphere at all. These scenes have all of the normal radiative qualities without the effects of atmospheric attenuation and path radiance. Such scenes were generated to be used as "truth" to compare the atmospheric compensation algorithms to an idealized no-atmosphere scene. The atmosphere used here was MODTRAN's mid-latitude summer.

Two different scenes were produced using DIRSIG, a strong plume case and a weak plume case. The strong plumes have a release rate of 50 g/s and contains regions where the plume is optically thick. The weak plumes have a release rate of 0.25 g/s and are everywhere optically thin. The strong plume release rate is akin to an industrial accident whereas the weak plumes are closer to actual factory release rates. Two different plumes were generated in each scene. One plume contained the atmospherically native gas ammonia. The other plume was of freon-114. Freon-114 was chosen because the gas has a strong feature in the 11.73 μm water vapor band used by the atmospheric compensation algorithms. The gas absorption spectra were taken from a standard library of laboratory-measured species.

Before any atmospheric compensation was performed or any comparison to the "truth" scene, noise was added to all the scenes. The noise was artifically developed to be spectrally correlated and resemble noise simular to what would produced by the SEBASS sensor. Figure 1 shows a single-band image of the strong plume case at 10.73 μmfor the strong plume case with no compensation.

3.2. Metrics

Two different metrics were selected to measure the effects of the AAC and ISAC algorithms. The results of the two algorithms were also compared to the uncompensated version of the image. The results of both the metrics

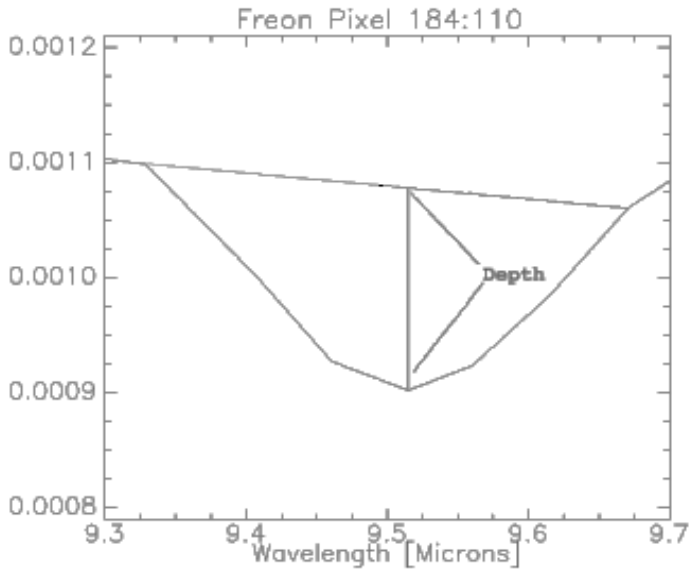

Figure 2. To calculate the feature depth a line is fit to the edges of the gas feature. The difference between the linear fit and the data is the feature strength. This example is taken of the Freon gas plume in the strong plume case as compensated by AAC.

are shown as distributions on a per pixel basis. This proved to be the most telling representation of the results.

3.2.1. Spectral Angle

The first metric used was the spectral angle. The spectrum of a pixel can be thought of as a multidimensional vector, where each band contributes a dimension. From the scalar product operation the angle between two such pixel spectra can be computed. Here, the spectral angle was calculated between one of the three atmospheric images and the image with no atmosphere on a per pixel basis. That is, for each plume pixel in each of the atmospheric images the spectral angle between the same spatial pixel in the no atmosphere image was found. The spectral angle is computed as

$$\theta(x) = \arccos\left(\frac{\mathbf{A}(x) \cdot \mathbf{B}(x)}{AB}\right) \tag{2}$$

where θ is the spectral angle as a function of pixel location, $\mathbf{A}$ is the pixel spectrum from an image with an atmosphere, and $\mathbf{B}$ is the spectrum of the same pixel in the truth image.

The spectral angle metric is most useful in describing how well the shape of a pixel spectrum matches the shape of another. It was used as a first pass at describing the performance of the algorithms. The shape of the pixel spectrum itself is not in general of direct importance to the gas plume quantification problem, so the usefulness is limited.

3.2.2. Feature Depth Metric

The second metric used was the feature depth metric. This metric makes direct comparison between the feature strength of the atmosphere-image pixels to the truth-image pixels. The feature depth is evaluated by means of a linear fit to the known edges of the particular gas feature (Figure 2). At the maximum absorbance of the feature a perpendicular is dropped from the linear fit to the spectral value of that band. The magnitude of this perpendicular is the feature depth or strength. Because the gas can be in either absorbtion or emission this feature depth can be either positive or negative. The edges of the feature and the maximum are known from the lab spectra.

The feature depth proved to be the more telling of the two metrics. The depth of the gas feature is directly related to the concentration path length and therefore of utmost importance to the problem of quantifying the

gas. A negative error corresponds to a feature depth that is too strong compared to the truth. A positive error corresponds to a feature depth that is too weak. This is true for pixels where the plume is in emission or absorption. Examples of the compensated and uncompensated features are shown in Figure 3. The freon feature is from 9.32 μm to 9.67 μm. The ammonia feature is from 10.68 μm to 10.86 μm.

4. RESULTS

Figures 4 & 5 show the results of the spectral angle comparison. If ISAC and AAC performed perfectly the spectral angle for all the pixels would be zero. The distributions show that in all cases ISAC and AAC have more pixels with a spectral anlge of zero than the uncompensated image. Effectively the distributions have been shifted closer to the "truth." For the ammonia plume in both the strong and weak case AAC "pushed" some of the pixels farther away from the "truth."

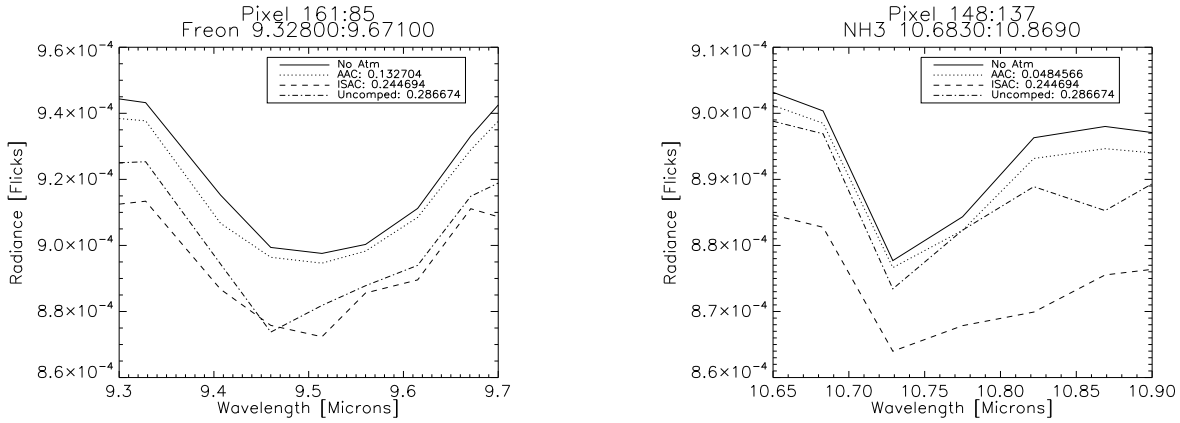

(a) **(b)**

Figure 3. Two different on-plume pixels showing gas features for all four cases for the strong plume. For each compensation method, the spectral angle between the pixel and the no-atmosphere "truth" scene is noted in the legend. (a) Freon plume (b) Ammonia plume

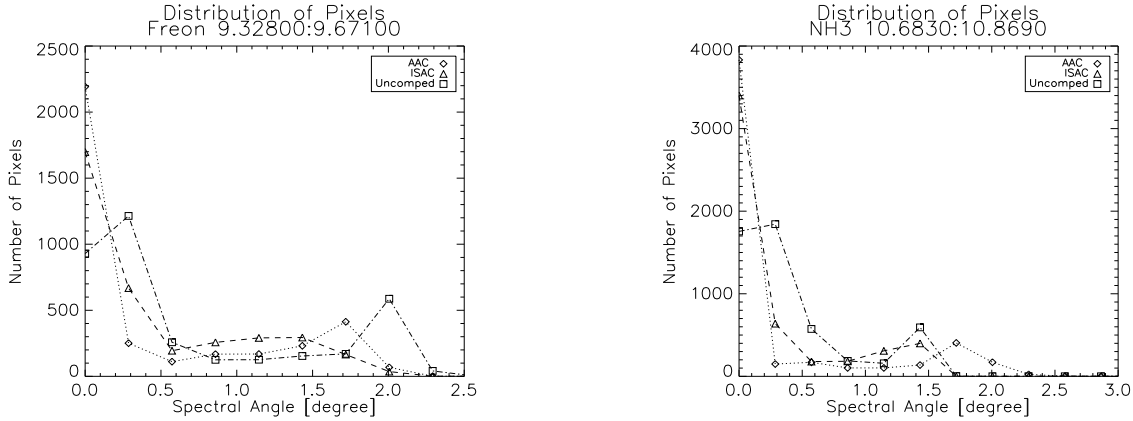

(a) **(b)**

Figure 4. Distribution of spectral angle for the strong plume case. Ideally ISAC & AAC should have a spectral angle of zero for all pixels. (a) Freon plume (b) Ammonia plume

Figures 6, 7, & 8 are the results of the feature depth metric. They show the distribution of pixels in terms of the relative error of the feature depth to the "truth." For freon two features were looked at. The first was freon's

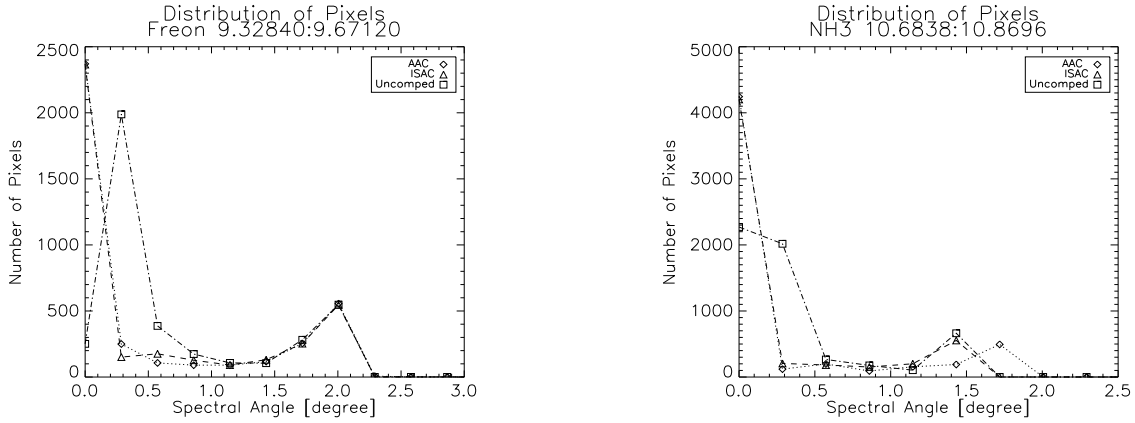

(a) **(b)**

Figure 5. Distribution of spectral angle for the weak plume case. (a) Freon plume (b) Ammonia plume

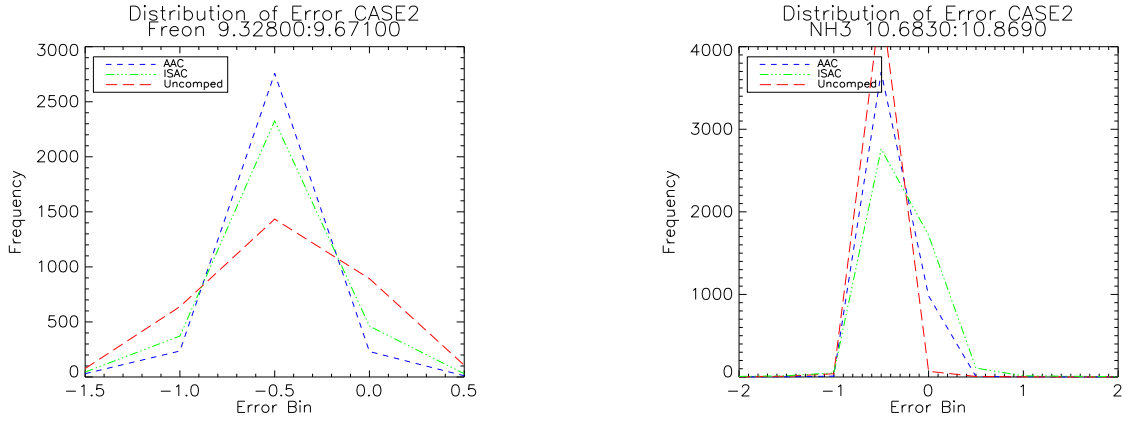

(a) **(b)**

Figure 6. Strong plume case results of the feature depth. The error is the relative error. (a) Freon plume (b) Ammonia plume

strongest absroption feature at 9.51 microns. The second feature is at 11.75 microns. This feature was chosen because it is close to the 11.73 μm water vapor band that both ISAC and AAC use to calculate the atmospheric parameters. A positive error corresponds to a feature that is too strong and a negative error corresponds to a feature that is too weak. All three atmospheric compensation methods overestimate the strength of the gas feature. Also, AAC's distribution changed dramatically from the shape of the uncompensated distribution when compare to ISAC, but only for the weak case of the freon plume and even than the effect is modest.

5. CONCLUSIONS

The purpose of this experiment was to quantitatively evaluate the performance of the thermal atmospheric compensation algorithms as to their impact on gas plume spectral features. In particular, the aim was to answer the question of whether or not to compensate an image before processing for the quantification of gaseous effluents. The two atmospheric algorithms studied were ISAC and AAC. The study was carried out on synthetic data for two different plume cases.

In comparison of the distributions of all the cases of all of the three preprocessing techniques it is found that there is little information about the feature depth gained from atmospheric compensation. The two algorithms failed to significantly change the distribution, expect in the weak case of the freon. This was a modest effect

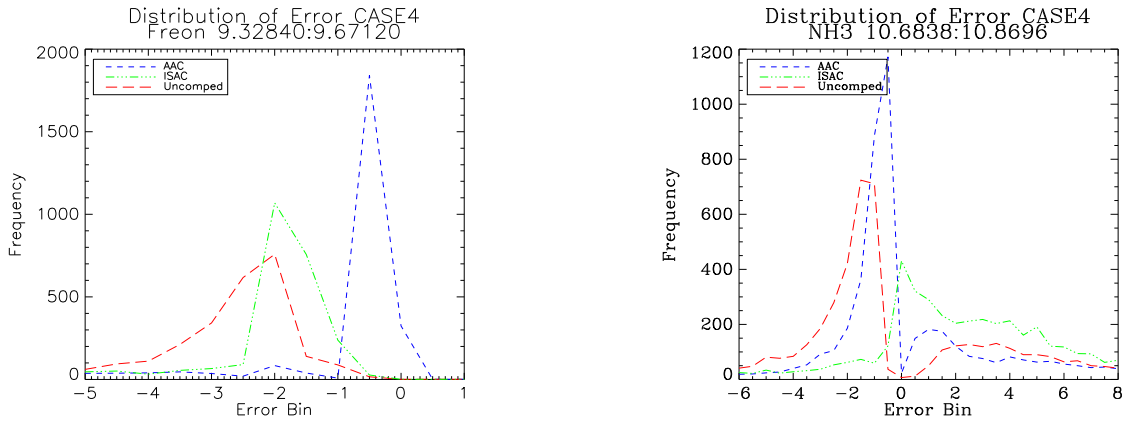

(a) **(b)**

Figure 7. Weak plume case results of the feature depth. The error is the relative error. (a) Freon plume (b) Ammonia plume

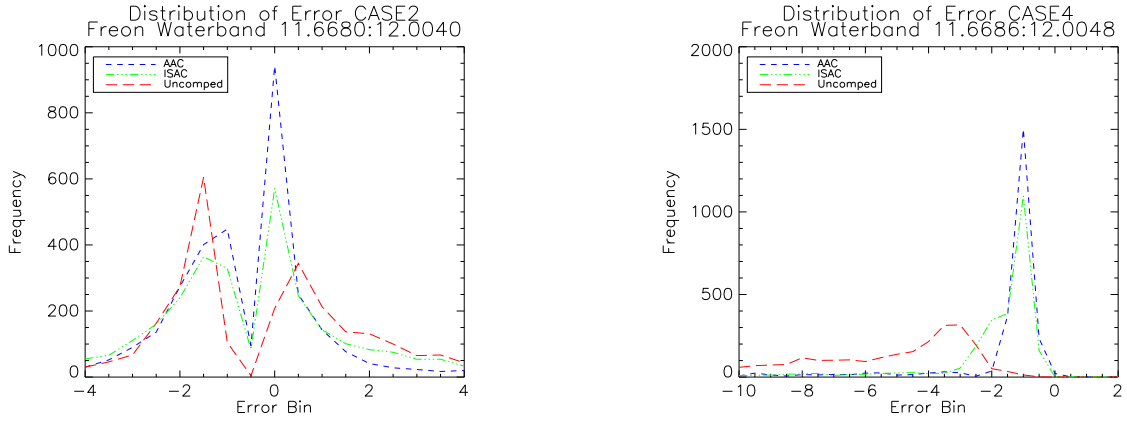

(a) **(b)**

Figure 8. Freon results at the 11.73 μm water vapor band. The error is the relative error. (a) Strong case (b) Weak case

though and is probably related to the spectral overlap of freon in the water vapor band. Given the small effect of atmospheric compensation on the feature depth, coupled with the overall uncertainty associated with any preprocessing, atmospheric compensation is not seen as useful in the area of the gas plume problem.

REFERENCES

1. E. O'Donnell, D. Messinger, C. Salvaggio, and J. Schott, "Identification and detection of of gaseous effluents from hyperspectral imagery using invariant algorithms," in *Algorithms and Technologies for Multispectral, Hyperspectral, and Ultraspectral Imagery X, Proceedings of SPIE, v. 5425*, S. Shen, ed., pp. 573 – 582, 2004.
2. D. Pogorzala, D. Messinger, C. Salvaggio, and J. Schott, "Gas plume species identification by regression analyses," in *Algorithms and Technologies for Multispectral, Hyperspectral, and Ultraspectral Imagery X, Proceedings of SPIE, v. 5425*, S. Shen, ed., pp. 583 – 591, 2004.
3. D. Messinger, "Gaseous plume detection in hyperspectral images: a comparison of methods," in *Algorithms and Technologies for Multispectral, Hyperspectral, and Ultraspectral Imagery X, Proceedings of SPIE, v. 5425*, S. Shen, ed., pp. 592 – 603, 2004.
4. S. Young. Aerospace Corporation, RAND Communication, 2002.
5. N. Gallagher, B. Wise, and D. Sheen, "Estimation of trace vapor concentration-pathlength in plumes for remote sensing applications from hyperspectal images," *Analytica Chimica Acta* **490**, pp. 139 – 152, 2003.
6. R. Czerwinski, K. Farrar, G. M.K., and J. Kerekes, "Spectral quality requirements for effluent quantification," in *Algorithms and Technologies for Multispectral, Hyperspectral, and Ultraspectral Imagery X, Proceedings of SPIE, v. 5425*, S. Shen, ed., pp. 616 – 627, 2004.
7. S. Young, B. Johnson, and J. Hackwell, "An in-scene method for atmospheric compensation of thermal hyperspectral data," *J. Geo. Res.* **107**(D24), pp. 14–1 – 14–20, 2002.
8. J. Hackwell, D. Warren, R. Bongiovi, H. S.J., T. Hayhurst, D. Mabry, M. Sivjee, and J. Skinner, "Lwir/mwir imaging hyperspectral sensor for airborne and ground-based remote sensing," in *Imaging Spectrometry II, Proceedings of SPIE, v. 2819*, M. Descour and J. Mooney, eds., pp. 102 – 107, 1996.
9. D. Gu, A. Gillespie, A. Kahle, and F. Palluconi, "Autonomous atmospheric compensation (aac) of high resolution hyperspectral thermal infrared remote-sensing imagery," *IEEE Trans. Geo. Rem. Sens.* **38**(6), pp. 2257 – 2570, 2000.
10. J. Schott, S. Brown, R. Raqueño, H. Gross, and G. Robinson, "An advanced synthetic image generation model and its application to multi/hyperspectral algorithm development," *Can. J. Rem. Sen.* **25**(2), pp. 99–111, 1999.
11. A. Berk, L. Bernstein, and D. Robertson, "Modtran: A moderate resolution model for lowtran 7.," Tech. Rep. GL-TR-89-0122, Air Force Geophysics Laboratory, Hanscom AFB, MA, 1988.
12. S. Kuo, J. Schott, and C. Chang, "Synthetic image generation of chemical plumes for hyperspectral applications," *Opt. Eng.* **39**(4), pp. 1047–1056, 2000.